The International Journal of **Medical Robotics** and **Computer Assisted Surgery**

THE INTERNATIONAL JOURNAL OF MEDICAL ROBOTICS AND COMPUTER ASSISTED SURGERY
Int J Med Robotics Comput Assist Surg 2016; **12**: 219–230.
Published online 15 July 2015 in Wiley Online Library (wileyonlinelibrary.com) **DOI:** 10.1002/rcs.1680

ORIGINAL ARTICLE

Experimental evaluation of co-manipulated ultrasound-guided flexible needle steering

Momen Abayazid[1*]
Claudio Pacchierotti[2]
Pedro Moreira[1]
Ron Alterovitz[3]
Domenico Prattichizzo[2]
Sarthak Misra[1,4]

[1]*MIRA-Institute for Biomedical Technology and Technical Medicine, Department of Biomechanical Engineering, Surgical Robotics Laboratory, University of Twente, Enschede, The Netherlands*

[2]*Department of Information Engineering and Mathematics, University of Siena, and with the Department of Advanced Robotics, Istituto Italiano di Tecnologia, Italy*

[3]*Department of Computer Science, University of North Carolina at Chapel Hill, USA*

[4]*Department of Biomedical Engineering, University of Groningen and University Medical Centre, Groningen, The Netherlands*

*Correspondence to: Momen Abayazid, Faculty of Engineering Technology, Department of Biomechanical Engineering, Postbus 217, 7500 AE, Enschede, The Netherlands.
Email: m.abayazid@utwente.nl

Accepted: 16 May 2015

Abstract

Background A teleoperation system for bevel-tipped flexible needle steering has been evaluated. Robotic systems have been exploited as the main tool to achieve high accuracy and reliability. However, for reasons of safety and acceptance by the surgical community, keeping the physician tightly in the loop is preferable.

Methods The system uses ultrasound imaging, path planning, and control to compute the desired needle orientation during the insertion and intuitively passes this information to the operator, who teleoperates the motion of the needle's tip. Navigation cues about the computed orientation are provided through haptic and visual feedback to the operator to steer the needle.

Results The targeting accuracy of several co-manipulation strategies were studied in four sets of experiments involving human subjects with clinical backgrounds.

Conclusions Experimental results show that receiving feedback regarding the desired needle orientation improves the targeting accuracy by a factor of 9 with respect to manual insertions. Copyright © 2015 John Wiley & Sons, Ltd.

Keywords ultrasound-guidance; needle steering; haptics; shared control

Introduction

Needle insertion into soft-tissue is a minimally invasive procedure used for diagnostic and therapeutic purposes. Examples of diagnostic needle insertion procedures are liver, kidney and lung biopsies to detect tumors (1). Therapeutic applications of needle insertion include brachytherapy of cervical, prostate, breast cancers, and also thermal ablation therapies such as cryotherapy (2). Imaging modalities such as ultrasound, magnetic resonance (MR), and computed tomography (CT) are often used during needle insertion procedures to accurately determine the needle and target positions (3). Inaccurate placement of the needle may result in misdiagnosis or unsuccessful treatment.

Flexible needles were introduced to provide enhanced steering capabilities, allowing the needle to avoid obstacles and accurately reach the target position (4). Flexible needles fabricated with an asymmetric tip (e.g. bevel tip) naturally deflect during insertion into soft-tissue (5). This can be exploited to make the needles move in non-straight paths and reach specified target positions (4). The path of a bevel-tip steerable needle in soft tissue can be predicted using the nonholonomic kinematics of a bicycle or unicycle model (5,6). The needle deflection can also be controlled using duty-cycling of the needle during insertion (7). This approach varies the needle curvature by changing the ratio between the period of needle insertion with spinning to the total period of insertion.

Due to the nonholonomic kinematics, accurately steering an asymmetric-tip needle to a target is challenging (4). Control algorithms can facilitate accurate needle placement. Several research groups have developed flexible needle deflection models for needle steering (4). Hauser *et al*. developed a 3D feedback controller that steers the needle along a helical path, although results were evaluated only in simulations (8). Abayazid *et al*. presented an autonomous two-dimensional (2D) ultrasound image-guided steering system, and a 3D robotic system in which they used both Fiber Bragg Grating sensors and ultrasound for feedback (9–11).

In the aforementioned studies, the needle steering was performed autonomously and the operator did not intervene during insertion. The main advantage of autonomous robotic systems is providing a significantly higher accuracy with respect to that of manual insertions. However, autonomous systems are not currently widely accepted by the clinical community due to concerns about safety (12,13). For this reason, Hungr *et al*. developed an autonomous robotic system that switches to manual mode in the case of predefined emergency conditions (14). Majewicz and Okamura presented a teleoperated system in which the operator commands the desired position in Cartesian space and the system provides force feedback that represents kinematic constraints and the position error of the robot. The evaluation of the system was based on simulations performed by an operator (15). Romano *et al*. presented a robotic system in which clinicians directly control the insertion and orientation of the needle using a 6-DOF haptic device (13). Finally, other researchers guarantee the insertion system safety using force feedback techniques (16,17).

Haptic feedback for shared control

Robotic teleoperation systems for medical procedures can enable high accuracy and repeatability while providing physicians with a level of manual control. Robotic teleoperation systems are composed of a slave robot, which interacts with a remote environment, and a master system, operated by a human (Figure 1). The slave robot is in charge of reproducing the movements of the operator, who in turn, needs to observe the operative environment with which the robot is interacting. This is possible through different types of information that flow from the remote scenario to the operator. They are usually a combination of visual and haptic stimuli. Visual feedback is already employed in commercial robotic surgery systems (e.g. the da Vinci Si Surgical System, Intuitive Surgical, Sunnyvale, CA, USA) while it is not common to find commercially-available devices implementing haptic force feedback. One of the few examples is the Sensei robotic catheter system (Hansen Medical, Mountain View, CA, USA).

However, haptic feedback is widely considered to be a valuable navigation tool during teleoperated surgical procedures (15,18,19). It enhances clinicians' performance in terms of completion time of a given task (20), accuracy (21), peak and mean applied force (18,20,22). In medicine, haptic feedback has been shown to improve performance in fine microneedle positioning (23), telerobotic catheter insertion (24), suturing simulation (25), cardiothoracic procedures (26), and cell injection systems (27). Wagner *et al*. (22), for example, examined the effect of haptic force feedback on a blunt dissection task and showed that system performance improved up to 150% in comparison with providing no force feedback, while also decreasing the number of tissue damaging errors by a factor of >3. Pacchierotti *et al*. presented preliminary results of a needle steering system that provides the operator with only vibratory feedback (28). Experiments were performed using a limited number of subjects and no path planning was implemented for obstacle avoidance. Other studies have linked the lack of significant haptic feedback to increased intra-operative injury in minimally invasive surgery operations (29) and endoscopic surgical operations (30). Moreover, haptic feedback can prevent undesirable trauma and incidental tissue damage, as it relays surgical tool–tissue interaction forces to the operator.

Haptic feedback can also be employed to *augment* the operating environment, providing additional valuable information to the operator, such as navigation cues. For example, Nakao *et al*. (31) presented a haptic navigation method that allows an operator to avoid collision with forbidden regions during surgery. It employs kinesthetic feedback through a 2D master manipulator. More recently, Ren *et al*. (32) implemented dynamic 3D virtual constraints with haptic and visual feedback during minimally invasive beating-heart procedures.

In addition to these approaches, which mostly involve kinesthetic force feedback, there is also a growing interest in *vibratory* feedback. Van Erp *et al*. (33), for instance, employed a vibrating waist belt to provide navigation information to the operator. Results indicated

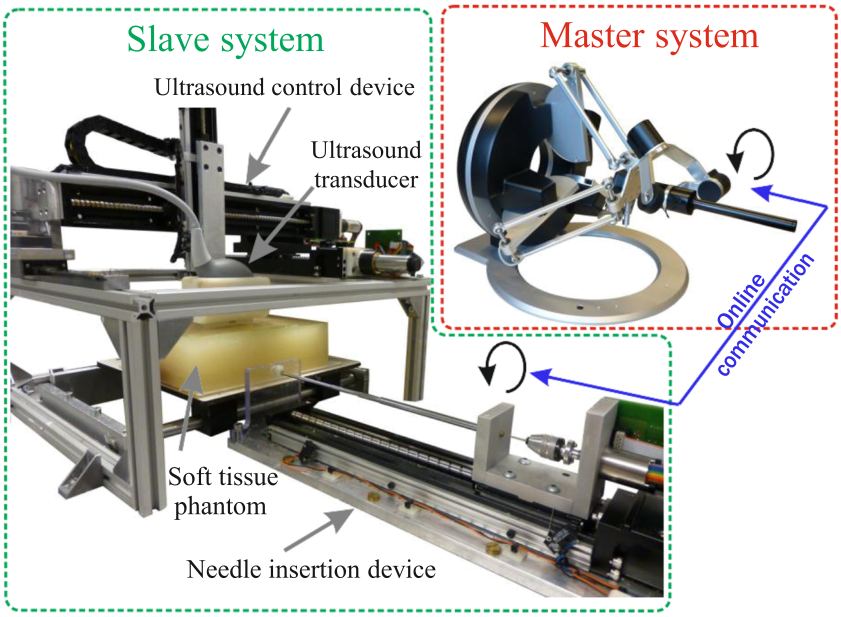

Figure 1. The slave system includes the needle control device for needle insertion and rotation about its axis, and also the ultrasound control device used for three-dimensional needle tip tracking. The master system includes the haptic device that allows the operator to control the needle

the usefulness of vibratory cues for navigation purposes as well as for situational awareness in multi-task environments. Lieberman *et al*. (34) presented a robotic suit for improved human motor learning. It provided vibratory feedback proportional to the error between the effective and learned motion. Schoonmaker and Cao (35) demonstrated that vibratory stimulation is a viable substitute for force feedback in minimally invasive surgery, enhancing operators' ability to control the forces applied to the tissue and differentiate its softness in a simulated tissue probing task. More recently, McMahan *et al*. (36) developed a sensing and actuating device for the da Vinci S Surgical System able to provide vibrotactile feedback of tool contact accelerations. Eleven surgeons tested the system and expressed a significant preference for the inclusion of vibratory feedback.

Contributions

In this study, we combine the advantages of manual steering with the high accuracy of autonomous (robotic) needle insertion. The proposed system enables operators to control the needle rotations while receiving navigation feedback from the path planning and control algorithms. In previous studies, haptic feedback was used mainly for avoiding collisions, conveying kinematic constraints or sensing tissue stiffness (15,18,37). To the best of our knowledge this is the first study to use vibratory and visual feedback to give the operator navigation cues using an ultrasound-guided system with an intra-operative path planner. Such types of feedback do not limit the operator's freedom of moving and controlling the haptic device as in the case of force feedback. We carry out several experiments that allow an operator to control the needle orientation using different combinations of visual and vibratory feedback as computed by the path planning and control algorithms. The subjects are provided with an online 3D view of the needle, target and obstacle positions to comprehend the system and its operating environment during the insertion procedure. The term 'visual feedback' refers to the navigation cues, while the term 'online 3D view' indicates displaying the overall operating environment.

We also attempt to employ subjects with a clinical background to be able to experimentally compare the case of manual control with the case of receiving navigation cues from the control algorithm under the same experimental conditions. This comparison will show the significance of using a co-manipulated needle steering system to improve the targeting accuracy. Different types of needle co-manipulation conditions, where the control algorithm assists the subject to steer the needle, are performed to assess which achieves the highest degree of accuracy and safety. The block diagram depicted in Figure 2 shows the algorithms forming the steering system to highlight the main contributions of this study. In the current study, we combine teleoperated control with path planning to steer the needle toward a target while avoiding two obstacles.

DOI: 10.1002/rcs

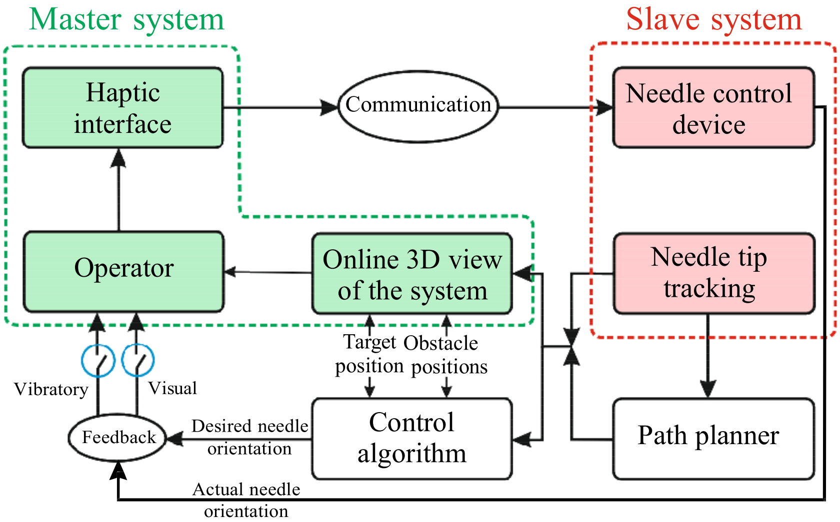

Figure 2. Through the Omega 6 haptic device, the operator controls the motion of the slave robot and, thus, the needle. The needle tracking system provides the control algorithm and path planner with the needle tip pose. An online three-dimensional (3D) view of the needle path, position and orientation, together with the target and obstacles positions, is displayed to the operator on a computer screen. The control algorithm computes the desired needle orientation to allow the needle to move along the planned path. The difference between the actual and the desired needle orientations is provided to the operator with visual or vibratory feedback. The feedback system loops every 40 ms, and the planned path is updated every second

Materials and methods

Slave system

The slave system includes the needle control device and the transducer control device. They are in charge of the needle tip tracking, control and path planning.

Needle tip tracking

Ultrasound imaging is used to track the needle tip in 3D-space during insertion. The resolution of the ultrasound image obtained is 0.12 mm per pixel. A 2D ultrasound image plane is positioned perpendicular to the insertion direction at the needle tip (see Figure 3). The transducer moves along the needle path during insertion to keep the tip in its field-of-view. It uses a closed loop control system based on a proportional-derivative algorithm that minimizes the error between the transducer scanning velocity and the needle insertion velocity, which is obtained from the slave robot's controller. Furthermore, a Kalman observer is implemented to minimize the influence of noise on the states of location and velocity of the needle tip and to predict subsequent states according to the needle tip velocity (38).

Finally, basic image processing techniques, such as median blur, thresholding, erosion and dilation are applied on ultrasound images intra-operatively. This increases the contrast between the tip and the surrounding phantom, preventing false tip detections. After that, the system computes the needle centroid location using image moments. The centroid represents the $y-z$ coordinates of the needle tip as shown in Figure 3 while the insertion (x) coordinates are obtained from the motor encoders of the ultrasound transducer control device.

The controller provides an accuracy in estimating the needle tip pose up to 0.64 mm and 2.68° for position and orientation, respectively. Further details on the tracking algorithm have been presented by Vrooijink *et al.* (39).

Path planning and control algorithms

We use a 3D path planning algorithm to generate a trajectory for the needle to reach a target while avoiding obstacles in a 3D environment (40,41). Using the information obtained from ultrasound images, the system provides the subjects with navigation cues to steer the needle along the planned path using the control algorithm. The needle path is planned using a customized version of the rapidly-exploring random tree (RRT) algorithm, which is a sampling-based method for path planning (42). To enable fast performance, our path planner effectively utilizes the needle's kinematics model and makes use of reachability-guided sampling for efficient expansion of the search tree. The planner is sufficiently fast that it can be executed in a closed-loop manner, updating the path every second. This closed-loop execution can enable the system to compensate for disturbances such as target and

DOI: 10.1002/rcs

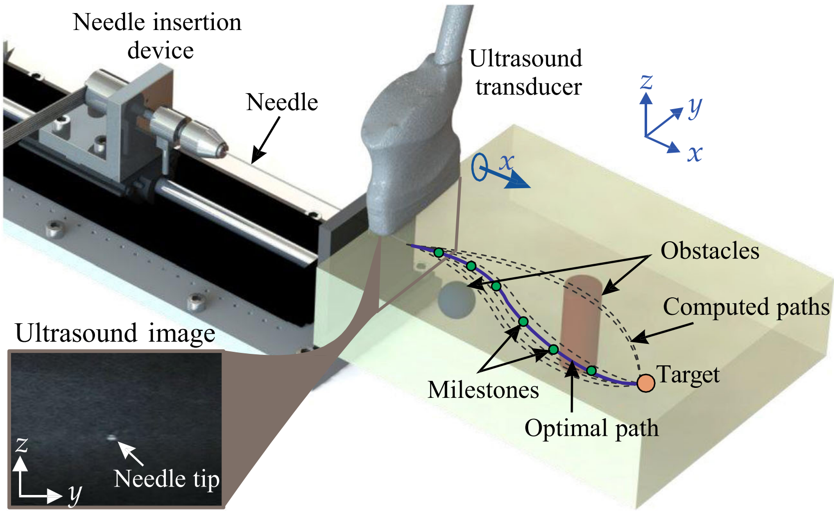

Figure 3. The needle tip pose is determined in three-dimensional space using a two-dimensional ultrasound transducer positioned to visualize the needle tip where the ultrasound image plane is perpendicular to the needle insertion axis (*x*-axis). The path planning algorithm generates a feasible path by exploring the state space using a rapidly exploring random tree. The path planner generates milestones along the path, and the control algorithm steers the needle using the milestones to move along the planned trajectory

obstacle motions (11). We refer the reader to Patil *et al*. for additional details on the planning algorithm (40).

Given pre-operative medical images, the operator can specify the insertion location, the target location, and the geometry of obstacles, which can include sensitive structures such as glands or blood vessels as well as impenetrable structures such as bones. After specifying the entire environment, the path planner computes a path that (1) reaches the target, and (2) is feasible, i.e. it avoids obstacles. The output of the path planning algorithm is a sequence of milestones along the path. The control algorithm computes the desired orientation that allows the subject to steer the needle toward the first milestone. As soon as a milestone is reached, the control algorithm computes the desired orientation to steer the needle toward the next milestone along the path.

The needle tip pose (position and orientation) obtained from the tracking algorithm is the main input of the control algorithm. First, the control algorithm estimates the region that the needle tip can reach during insertion. The controller then computes intra-operatively the needle tip desired orientation every 40 ms to follow the planned trajectory and reach the target. As mentioned before, the needle can be assumed to move along arcs during its insertion into a soft-tissue phantom (5). The direction of each arc depends on the bevel tip orientation, which is controlled by rotating the needle about its insertion axis (Figure 3). Additional details about the control algorithm can be found in the work of Abayazid *et al*. (9,11).

Master system

The master system is responsible for both steering the slave robot and displaying navigation cues regarding the desired needle orientation. Navigation cues allow co-manipulation between the subject (operator) and robotic system for needle steering. In order to avoid confusion and consequent possible errors in the medical intervention, the meaning of such cues must be easy to understand.

In this study, we propose to provide the subject with (1) an online 3D view of the system that includes the needle path, needle tip location, obstacle locations and target location, and (2) visual and vibratory feedback about the desired orientation of the needle as evaluated by the control algorithm described in the section 'Path planning and control algorithms'. Details on how visual and vibratory feedback are provided to the subject are reported in sections 'Visual feedback' and 'Vibratory feedback', respectively.

Setup

The master system consists of two computer screens and a single-contact grounded haptic interface Omega 6 (Force Dimension, Nyon, Switzerland), as shown in Figures 1 and 4. It provides the subject with navigation cues through visual and/or vibratory feedback, according to the feedback condition being considered (see section 'Slave system'). The needle is inserted automatically with a constant velocity while the haptic interface allows the

DOI: 10.1002/rcs

subject to control the orientation of the needle during insertion. In fact, the needle orientation is actuated to match the orientation of the pen-shaped haptic probe controlled by the subject.

Visual feedback

Two straight line segments, one red and one yellow, are presented to the subject on a computer screen (see Figure 4). The position of one of the end points of the lines is fixed, while the other one moves on a circumference whose center is the fixed end point and whose radius is the length of the segments. The coordinates of the moving end points with respect to the center of the circumference are (cos θ_i, sin θ_i) and (cos θ, sin θ) for the red and yellow line, respectively, where angles $\theta_i(t)$ and $\theta(t)$ are the desired and current orientation of the needle, respectively. The red and yellow lines thus represent the desired and current axial orientation of the needle tip, respectively. The subject is asked to align the yellow line with the red one, since a perfect alignment of the lines denotes the least deviation from the computed plan.

Vibratory feedback

Vibratory feedback is controlled by a penalty function based on the difference between the desired orientation $\theta_i(t)$ and the current orientation $\theta(t)$ of the needle:

$$f_v = A_1|\theta_i(t) - \theta(t)|\,\mathrm{sgn}(\sin(2\pi f t)) \tag{1}$$

where

$$A_1 = \frac{3}{\pi} I_{3\times1} N/rad$$

and

$$f = \begin{cases} 100\ Hz & if\ \theta(t) - \theta_i(t) \geq 0, \\ 25\ Hz & if\ \theta(t) - \theta_i(t) < 0. \end{cases}$$

Vibrations thus provide information about the desired orientation $\theta_i(t)$, indicating in which direction and how much the subject should rotate the pen-shaped haptic probe. Frequency ω indicates in which direction the subject should rotate the pen-shaped haptic probe: clockwise for f= 100 Hz and counter-clockwise for f= 25 Hz. Frequency values are chosen to maximally stimulate the Pacinian corpuscle receptors (43), be easy to distinguish (44) and fit the master device specifications. On the other hand, the amplitude of these vibrations indicates how much the subject should rotate the haptic probe: no vibrations indicate the best performance. Amplitude scaling matrix A_1 is chosen to maximize the just-noticeable difference (45) for the error $|\theta_i(t) - \theta(t)|$ and fit the master device specifications.

Experiments

The aim of the experiments is to investigate the co-manipulation configurations that achieve sufficient targeting accuracy. We attempt to combine the advantages of manual insertion with the high accuracy of autonomous (robotic) needle insertion.

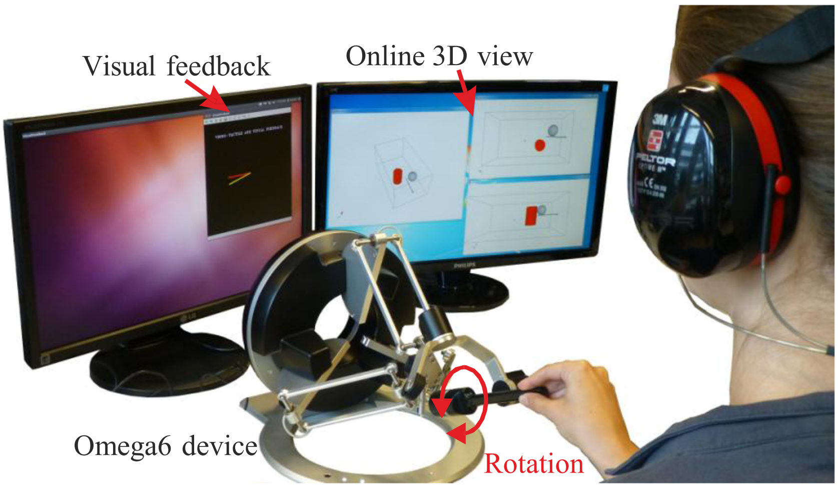

Figure 4. Experimental evaluation. The subject performs an experimental trial while receiving both visual and vibratory feedback (VI +VB). The subject is asked to follow the online three-dimensional (3D) view of the system on the right screen and the visual feedback on the left screen

Experimental protocol

The experimental setup is shown in Figure 4. A 3D view of the planned path, target location, needle and obstacle positions using an isometric, top and side views is always displayed to the subject (right screen in Figure 4). The task consists of rotating the pen-shape haptic probe about its axis to steer the needle toward the target point while avoiding two obstacles. The needle insertion velocity is fixed to 1 mm/s and the target point is placed 85 mm from the insertion point. We used a Nitinol needle of 0.5 mm diameter and 30° bevel angle.

In the first three conditions, subjects receive visual and vibratory feedback from the control algorithm, in addition to the online 3D view of the system. In the last condition, subjects control the needle orientation relying only on the online 3D view. Each subject performs twelve randomized trials of the needle steering task, with three repetitions for each feedback condition proposed:

- visual feedback (VI) on the desired and current orientation of the needle, as described in section 'Visual feedback';
- vibratory feedback (VB) on the desired and current orientation of the needle, as described in section 'Vibratory feedback';
- visual and vibratory feedback (VI+VB) on the desired and current orientation of the needle;
- no feedback (N) from the control algorithm on the desired and current orientation of the needle except from the online 3D view.

Subjects

In order to determine the number of subjects needed for our research study, we ran a power analysis using the open source G*Power software (University of Kiel, Germany). The completion times for each trial were compared using a repeated-measures analysis of variance (ANOVA). Power analysis revealed that, in order to have a 90% chance of detecting differences in our data, we need at least 14 participants (partial $\eta^2 = 0.278$, effect size 0.621, actual power 0.918).

Fourteen subjects with medical background participated in the experiment (3 males, 11 females, age 24–32). The subjects were mainly senior technical medicine[1] students who had completed a training in clinical insertions and endoscopy. In addition, we enrolled one nurse with 5 years clinical experience in a hospital, and 3 biomedical engineers to perform the experiments. The subjects participated on a voluntary basis and signed an informed consent form. Subjects were informed about the procedure before the beginning of the experiment and a 5-minute familiarization period was provided to make them acquainted with the experimental setup. Subjects were asked to wear a pair of noise canceling headphones, and they did not have direct visual access to the needle control device (slave system) in order to prevent visual cues that might alter their judgment. Before each trial, subjects were informed about which experimental condition was going to be considered.

[1]Technical Medicine is a Masters level programme in which students learn to integrate advanced technologies within the medical sciences to improve patient care.

Results

In order to evaluate the accuracy of the system we test the targeting accuracy (the deviation of the needle tip from the target position). Safety is evaluated by detecting the insertions where the obstacles are hit by the needle. Efficiency is evaluated by testing (a) the orientation error between the actual orientation and the needle orientation computed by the control algorithm, (b) the completion time of the insertion, and (c) comparing the first three experimental cases while visual or/and vibratory feedback are provided to the subjects with the case where no visual nor vibratory feedback is provided to test the system efficiency. The completion time is also dependent on the path generated for a specific insertion. An optimized path is generated at the beginning of the insertion but as the user deviates the needle from the initial path, the online generated paths correct for these deviations and the insertion completion time is expected to increased.

We evaluate the mean error in reaching the target point e_t, the mean error over time in following the desired orientation signals e_o, and the completion time t_c. Error e_t is calculated as $\mathbf{n_f} - \mathbf{o_t}$, where $\mathbf{n_f} \in R^{3\times 1}$ represents needle tip position at the end of the task (see Table 1). Error in the desired orientation signals e_o is computed as the mean over time of $\theta(t) - \theta_i(t)$. Data resulting from different repetitions of the same condition, performed by the same subject, were averaged before comparison with other

Table 1. The targeting error is calculated as the absolute distance between the needle tip at the end of insertion and the center of the localized target. Its mean error is μ and its standard deviation is σ. The subject receives visual (VI), vibratory (VB), visual and vibratory (VI+VB), or no (N) feedback from the control algorithm

	VI	VB	VI+VB	N
μ (mm)	1.07	1.39	1.03	9.23
σ (mm)	0.59	0.70	0.64	6.68

DOI: 10.1002/rcs

conditions' data. Data have been transformed when necessary to meet the test's assumptions (46).

Figure 5(a) shows targeting error e_t for the four experimental conditions. The collected data passed the Shapiro-Wilk normality test. Mauchly's Test of Sphericity indicated that the assumption of sphericity had been violated ($\chi^2(2) = 105.054$, $P < 0.001$). A repeated-measure ANOVA with a Greenhouse-Geisser correction showed a statistically significant difference between the means of the feedback conditions ($F_{1.017,13.226} = 69.734$, $P < 0.001$, a = 0.05). Post-hoc analysis (Games-Howell post-hoc test) revealed a statistically significant difference between all the groups ($P < 0.001$). This means that conditions VI+VB and N performed, respectively, significantly better and worse than all the others. Condition VI outperformed condition VB.

Figure 5(b) shows orientation error e_o for the four experimental conditions. The collected data passed the Shapiro-Wilk normality test. Mauchly's Test of Sphericity indicated that the assumption of sphericity had been violated ($\chi^2(2) = 12.843$, $P = 0.025$). A repeated-measure ANOVA with a Greenhouse-Geisser correction showed a statistically significant difference between the means of the feedback conditions ($F_{1.741,22.628} = 83.849$, $P < 0.001$, a = 0.05). Post-hoc analysis (Games-Howell post-hoc test) revealed statistically significant difference between all the groups (VI vs VB, $P = 0.016$; VI vs VI+VB, $P = 0.035$; VI vs N, $P < 0.001$; VB vs VI+VB, $P < 0.001$; VB vs N, $P < 0.001$; VI+VB vs N, $P < 0.001$). As for Figure 5(a), this also means that conditions VI+VB and N performed, respectively, significantly better and worse than all the others. Condition VI outperformed condition VB.

Figure 5(c) shows the completion time t_c for the four experimental conditions. The collected data passed the Shapiro-Wilk normality test. Mauchly's Test of Sphericity indicated that the assumption of sphericity had been violated ($\chi^2(2) = 24.629$, $P < 0.001$). A repeated-measure ANOVA with a Greenhouse-Geisser correction showed a statistically significant difference between the means of the feedback conditions ($F_{1.380,17.942} = 16.440$, $P < 0.001$, a = 0.05). Post-hoc analysis (Games-Howell post-hoc test) revealed statistically significant difference between conditions N and all the others (VI vs N, $P = 0.013$; VB vs N, $P = 0.015$; VI+VB vs N, $P = 0.001$), and between conditions VB and VI+VB ($P = 0.009$). This means that subjects took significantly more time to complete the task while being provided with no feedback from the controller (condition N). On the other hand, subjects complete the task significantly faster in condition VI+VB than in condition VB.

In addition to the quantitative evaluation presented above, we also measured subjects' experience. Immediately after the experiment, participants were asked to fill in an 18-item questionnaire using bipolar Likert-type seven-point scales. It contained a set of assertions, where a score of 7 was described as 'completely agree' and a score of 1 as 'completely disagree' with the assertion. The evaluation of each question is reported in Table 2. Figure 6 shows the mean ratings given by

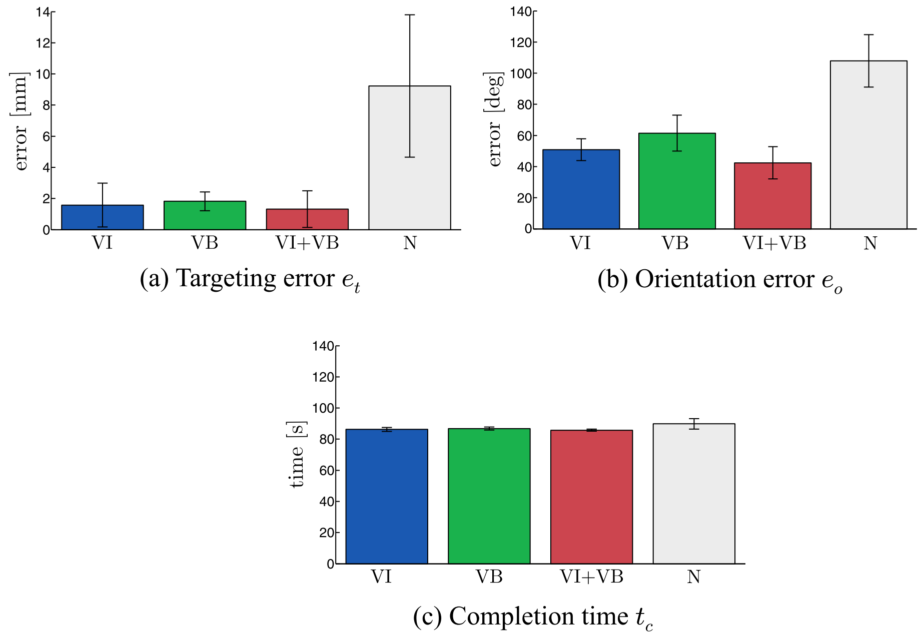

(a) Targeting error e_t

(b) Orientation error e_o

(c) Completion time t_c

Figure 5. Needle insertion experiment. Targeting error e_t, orientation error *eo*, and completion time t_c (mean and SD) are plotted for the experimental conditions where the subjects receive visual (VI), vibratory (VB), visual and vibratory (VI+VB), and no (N) feedback from the control algorithm. Lower values of these metrics indicate better performance in completing the given task

DOI: 10.1002/rcs

Table 2. Subjects' experience evaluation. Participants rated these statements, presented in random order, using a 7-point Likert scale (1 = completely disagree, 7 = completely agree). Means and standard deviations are reported for the visual (VI), vibratory (VB), visual-vibratory (VI+VB), and no feedback (VI) conditions

		Questions	Mean	σ
General	Q1	The system was intuitive.	3.36	1.08
	Q2	The system was easy to use.	3.79	0.70
	Q3	I needed support by the test administrator to be able to use the system.	2.50	1.16
	Q4	Most people would quickly learn how to use the system.	3.57	0.94
	Q5	I felt confident using the system.	3.00	1.11
	Q6	I needed more training to confidently use the system.	3.43	1.40
	Q7	Sound from the device caused disturbance while performing the experiments.	1.71	0.99
	Q8	I was well-isolated from external noises.	3.86	1.51
	Q9	At the end of the experiment I felt tired.	2.36	1.01
	Q10	I found useful to see the 3D representation of the needle insertion.	3.71	0.91
VI	Q11	In this feedback condition I performed the best.	3.76	1.12
	Q12	In this feedback condition I could pay attention to the 3D representation of the needle.	2.07	1.14
VB	Q13	In this feedback condition I performed the best.	3.29	0.99
	Q14	In this feedback condition I could pay attention to the 3D representation of the needle.	3.93	1.07
VI+VB	Q15	In this feedback condition I performed the best.	4.00	1.41
	Q16	In this feedback condition I could pay attention to the 3D representation of the needle.	2.21	1.19
N	Q17	In this feedback condition I performed the best.	1.71	1.14
	Q18	In this feedback condition I could pay attention to the 3D representation of the needle.	4.14	1.17

the subjects in eight questions of the post-experimental questionnaire. Figure 6(a) shows the ratings given by the subjects to the question 'In this feedback condition I performed the best' across the four different feedback conditions (Q11 vs. Q13 vs. Q15 vs. Q17, see Table 2). Since the data were registered at the ordinal level, we ran a Friedman test. Ratings were statistically significantly different for different feedback conditions, $\chi^2(3) = 18.378$, $P < 0.001$. Pairwise comparisons were performed with a Bonferroni correction for multiple comparisons. Ratings were statistically significantly different between condition N and all the others (VI vs N, $P = 0.013$; VB vs N, $P = 0.032$; VI+VB vs N, $P = 0.001$). This means that subjects felt that they performed significantly worse in condition N with respect to all the others. Figure 6(b) shows the ratings given to the question 'In this feedback condition I could pay attention to the 3D representation of the needle' across the four feedback conditions (Q12 vs. Q14 vs. Q16 vs. Q18, see Table 2). This question has been asked to evaluate the ability of the subject to monitor the overall insertion procedure using the 3D system view while performing the experiments. We ran again a Friedman test. Ratings were statistically significantly different across the feedback conditions, $\chi^2(3) = 21.095$, $P < 0.001$. Pairwise comparisons were performed with a Bonferroni correction for multiple comparisons. Ratings were statistically significantly different between conditions VI and VB ($P = 0.008$), VI and N ($P = 0.008$), VB and VI+VB ($P = 0.020$),

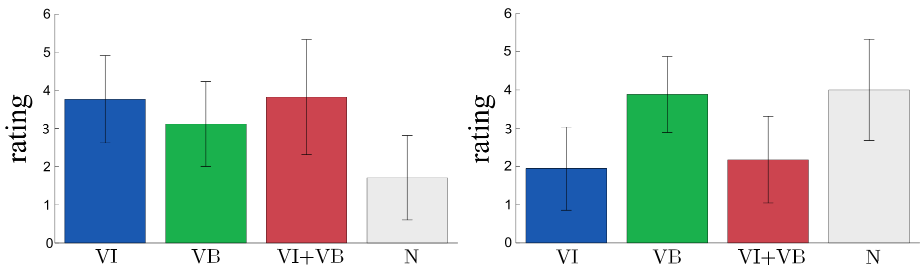

(a) In this feedback condition I performed the best. (Q11 vs. Q13 vs. Q15 vs. Q17, see Table 2)

(b) In this feedback condition I could pay attention to the 3D representation of the needle. (Q12 vs. Q14 vs. Q16 vs. Q18, see Table 2)

Figure 6. Questionnaire. Answers (mean and SD) are plotted for the experimental conditions in which the subjects receive visual (VI), vibratory (VB), visual and vibratory (VI+VB), and no (N) feedback from the control algorithm

DOI: 10.1002/rcs

VI+VB and N (P = 0.020). This shows that, as expected, providing the subjects with visual feedback about the desired orientation of the needle prevented them from focusing on the 3D view of the system (see Figure 3). On the other hand, conditions VB and N enabled the subjects to look at the 3D view of the system. Moreover, the needle hit an obstacle in 9 trials (out of 42) while receiving no navigation feedback from the control algorithm (N), while a collision never occurred while receiving any type of control feedback (VI, VB, or VI+VB).

Please refer to the accompanying video[2] *as supplementary material that demonstrates the experimental results*.

Discussion

Results show that all the subjects were able to steer the needle with an accuracy of 1 mm, while receiving feedback from the control algorithm. The mean targeting accuracy improved by a factor of 9 while receiving visual, vibratory or combined feedback with respect to the condition where no navigation feedback from the control algorithm was provided to the subjects. This shows that steering a bevel-tipped flexible needle is not trivial, and receiving an online 3D view of the system may not be sufficient for accurate steering.

According to our post-experiment questionnaire, subjects preferred visual feedback (VI) over vibratory feedback (VB). The reason could be that humans are more used to dealing with visual cues with respect to vibratory ones, and, therefore, they feel more comfortable with them. However, employing visual feedback did not give the subject the chance to follow the 3D system view. It was difficult for the subject to follow the online 3D view (to monitor the overall insertion procedure) while receiving visual feedback from the control algorithm about the desired and current orientation of the needle (VI and VI+VB) (Figure 3).

Conclusions

In this study, we present a teleoperation system to steer bevel-tipped flexible needles. An ultrasound-guided system with an intra-operative path planner is used to assist the subject to steer the needle tip toward a target while avoiding two obstacles. The system enables subjects to directly maneuver the surgical tool while providing them with navigation cues through visual and vibratory feedback. Fully autonomous medical robotic systems are still not totally accepted by the medical community due to safety reasons. For this reason, in our work, a control algorithm computes the desired needle orientation during insertion but the needle motion is directly controlled by the subject. The desired orientation is provided to the master interface, which presents it to the subject, who commands the slave robot and steers the needle to follow the planned path. Four experimental conditions are taken into account. Subjects control the needle orientation using visual, vibratory, visual and vibratory (combined) or no feedback from the control algorithm. In all conditions subjects are provided with an online 3D view of the needle, target and obstacle positions. A questionnaire is also filled in by the subjects to obtain feedback about their experience with different co-manipulation configurations.

Experimental results show that navigation cues provided by the control algorithm (VI, VB and VI+VB) improve the targeting accuracy with respect to the experimental condition where only the online 3D view is displayed (N) for the subject. This result confirms the hypothesis that bevel-tipped needles are difficult to steer manually without feedback. Although the targeting accuracy is similar for the three conditions with feedback from the control algorithm, the subjects felt more comfortable receiving visual feedback. However, they conclude that using vibratory feedback is convenient since it enables them to monitor the needle trajectory during the insertion.

The proposed system can be employed in prostate interventions using a transrectal transducer for ultrasound guidance where the needle should avoid the neurovascular bundles near the penile bulb (47). Furthermore, if we cannot place the ultrasound probe for needle tracking we can use other modalities such as electromagnetic tracking.

Future work

We will estimate the needle behavior during insertion in different inhomogeneous biological tissues. Since the proposed system received an initial acceptance by subjects with clinical background, advanced image processing algorithms will be implemented to track the needle tip in biological tissue to get the system closer to practice. Work is in progress to use kinesthetic force to provide subjects with force feedback regarding the mechanical properties of the tissue being penetrated. The visual feedback will be integrated in the same display of the online 3D view to make it easier for the subject to follow. Finally, the steering system can also be extended to detect patient movements that occur during needle insertion such as respiration and fluid flow.

[2]Video link: http://goo.gl/kFYsWt

DOI: 10.1002/rcs

Acknowledgements

The authors would like to thank Dr Sachin Patil for his earlier contributions in developing the path planning algorithm.

Conflict of interest

The authors have declared that there is no conflict of interest.

Funding

The research leading to these results has received funding from the Netherlands Organization for Scientific Research (NWO-Project: 11204) and from the European Union Seventh Framework Programme FP7/2007-2013 under grant agreement n° 270460 of the project 'ACTIVE - Active Constraints Technolo- gies for Ill-defined or Volatile Environments' and under grant agreement n° 601165 of the project 'WEARHAP - WEARable HAPtics for humans and robots'.

References

1. Boctor EM, Choti MA, Burdette EC, Webster RJ. Three-dimensional ultrasound-guided robotic needle placement: an experimental evaluation. *Int J Med Robot Comput Assist Surg* 2008; **4**: 180–191.
2. Beddy P, Rangarajan RD, Sala E. Role of MRI in intracavitary brachytherapy for cervical cancer: what the radiologist needs to know. *Am J Roentgenol* 2011; **196**: W341–W347.
3. Seifabadi R, Song SE, Krieger A *et al.* Robotic system for MRI-guided prostate biopsy: feasibility of teleoperated needle insertion and *ex vivo* phantom study. *Int J Comput Assist Radiol Surg* 2012; **7**: 181–190.
4. Cowan NJ, Goldberg K, Chirikjian GS *et al.* Surgical robotics. In Robotic Needle Steering: Design, Modeling, Planning, and Image Guidance. Springer: USA, 2011; 557–582.
5. Webster RJ, III, Kim JS, Cowan NJ *et al.* Nonholonomic modeling of needle steering. *Int J Robot Res* 2006; **25**: 509–525.
6. Park W, Kim JS, Zhou Y *et al*. Diffusion-based motion planning for a nonholonomic flexible needle model. Proceedings of the IEEE International Conference on Robotics and Automation. (*ICRA*), Barcelona, Spain, 2005; 4600–4605.
7. Engh JA, Podnar G, Khoo SY, Riviere CN. Flexible needle steering system for percutaneous access to deep zones of the brain. *Proceedings of the IEEE Annual Northeast Bioengineering Conference* (*NEBEC*), Easton, USA. 2006; 103–104.
8. Hauser K, Alterovitz R, Chentanez N *et al*. Feedback control for steering needles through 3D deformable tissue using helical paths. *Proceedings of Robotics*: *Science and Systems* (*RSS*), vol. 37, Seattle, USA, 2009.
9. Abayazid M, Roesthuis RJ, Reilink R, Misra S. Integrating deflection models and image feedback for real-time flexible needle steering. *IEEE Trans Robot* 2013; **29**: 542–553.
10. Abayazid M, Kemp M, Misra S. 3D flexible needle steering in soft- tissue phantoms using fiber bragg grating sensors. Proceedings of the IEEE International Conference on Robotics and Automation (*ICRA*), Karlsruhe, Germany, 2013; 5823–5829.
11. Abayazid M, Vrooijink GJ, Patil S, Alterovitz R, Misra S. Experimental evaluation of ultrasound-guided 3D needle steering in biological tissue. *Int J Comput Assist Radiol Surg*. 2014; **9**: 931–939.
12. Troccaz J, Peshkin M, Davies B. Guiding systems for computer-assisted surgery: introducing synergistic devices and discussing the different approaches. *Med Image Anal* 1998; **2**: 101–119.
13. Romano JM, Webster III RJ, Okamura AM. Teleoperation of steerable needles. Proceedings of the IEEE International Conference on Robotics and Automation (ICRA), Roma, Italy, 2007; 934–939.
14. Hungr N, Troccaz J, Zemiti N, Tripodi N. Design of an ultrasound- guided robotic brachytherapy needle-insertion system. Proceedings of the IEEE international conference on Engineering in Medicine and Biology Society (*EMBC*), Minneapolis, MN, USA, 2009; 250–253.
15. Majewicz A, Okamura AM. Cartesian and joint space teleoperation for nonholonomic steerable needles. World Haptics Conference (WHC), Daejeon, Korea, 2013; 395–400.
16. Schouten MG, Ansems J, Renema WKJ *et al*. The accuracy and safety aspects of a novel robotic needle guide manipulator to perform transrectal prostate biopsies. *Med Phys* 2010 September; **37**: 4744–4750.
17. Yakar D, Schouten MG, Bosboom DGH *et al.* Feasibility of a pneumatically actuated MR-compatible robot for transrectal prostate biopsy guidance. *Radiology January* 2011; **260**: 241–247.
18. Prattichizzo D, Pacchierotti C, Rosati G. Cutaneous force feedback as a sensory subtraction technique in haptics. *IEEE Trans Haptics November* 2012; **5**: 289–300.
19. Pacchierotti C, Abayazid M, Misra S, Prattichizzo D. Teleoperation of steerable flexible needles by combining kinesthetic and vibratory feedback. *IEEE Trans Haptics September* 2014; **7**: 551–556.
20. Meli L, Pacchierotti C, Prattichizzo D. Sensory subtraction in robot-assisted surgery: fingertip skin deformation feedback to ensure safety and improve transparency in bimanual haptic interaction. *IEEE Trans Biomed Eng* 2014; **61**: 1318–1327.
21. Pacchierotti C, Tirmizi A, Prattichizzo D. Improving transparency in teleoperation by means of cutaneous tactile force feedback. *ACM Trans Appl Perception (TAP)* 2014; **11**4: 1–4: 16.
22. Wagner CR, Stylopoulos N, Howe RD. The role of force feedback in surgery: analysis of blunt dissection. Proceedings of the Symposium of Haptic Interfaces for Virtual Environment and Teleoperator Systems, 2002; 68–74.
23. Salcudean SE, Ku S, Bell G. Performance measurement in scaled teleoperation for microsurgery. Proceedings of the First Joint Conference on Computer Vision, Virtual Reality and Robotics in Medicine and Medial Robotics and Computer-Assisted Surgery, Grenoble, France, 1997; 789–798.
24. Kazi A. Operator performance in surgical telemanipulation. *Presence: Teleoperators and Virtual Environments* 2001; **10**: 495–510.
25. Moody L, Baber C, Arvanitis TN *et al.* Objective surgical performance evaluation based on haptic feedback. *Studies Health Technol Inform* 2002; **85**: 304–310.
26. Kennedy CW, Hu T, Desai JP *et al.* A novel approach to robotic cardiac surgery using haptics and vision. *Cardiovasc Eng* 2002; **2**: 15–22.
27. Pillarisetti A, Pekarev M, Brooks AD, Desai JP. Evaluating the effect of force feedback in cell injection. *IEEE Trans Automat Sci Eng* 2007; **4**: 322–331.
28. Pacchierotti C, Abayazid M, Misra S, Prattichizzo D. Steering of flexible needles combining kinesthetic and vibratory force feedback. Proceeding of the IEEE Conference on Intelligent Robots and Systems (IROS), Chicago, USA, 2014; 1202–1207.
29. Okamura AM. Haptic feedback in robot-assisted minimally invasive surgery. *Current Opin Urol* 2009; **19**: 102–107.
30. Hashizume M, Shimada M, Tomikawa M *et al.* Early experiences of endoscopic procedures in general surgery assisted by a

computer-enhanced surgical system. *Surg Endosc* 2002; **16**: 1187–1191.
31. Nakao M, Imanishi K, Kuroda T, Oyama H. Practical haptic navigation with clickable 3D region input interface for supporting master–slave type robotic surgery. *Studies Health Technol Inform* 2004; **98**: 265–271.
32. Ren J, Patel RV, McIsaac KA, Guiraudon G, Peters TM. Dynamic 3-D virtual fixtures for minimally invasive beating heart procedures. *IEEE Trans Med Imag* 2008; **27**: 1061–1070.
33. van Erp JBF, van Veen HAHC, Jansen C, Dobbins T. Waypoint navigation with a vibrotactile waist belt. *ACM Trans Appl Percept* 2005; **2**: 106–117.
34. Lieberman J, Breazeal C. Tikl: development of a wearable vibrotactile feedback suit for improved human motor learning. *IEEE Trans Robot* 2007; **23**: 919–926.
35. Schoonmaker RE, Cao CGL. Vibrotactile feedback enhances force perception in minimally invasive surgery. *Proc Human Factors Ergonom Soc Annual Meeting* 2006; **50**: 1029–1033.
36. McMahan W, Gewirtz J, Standish D *et al.* Tool contact acceleration feedback for telerobotic surgery. *IEEE Trans Haptics* 2011; **4**: 210–220.
37. Ni D, Chan WY, Qin J *et al*. An ultrasound-guided organ biopsy simulation with 6D of haptic feedback. Med Image Comput Comput-Assist Intervent, vol. 11, Metaxas D, Axel L, Fichtinger G, Szkely G (eds), Springer: New York/Berlin/Heidelberg, 2008; 551–559.
38. Bar-Shalom Y, Li XR, Kirubarajan T. Estimation with Applications to Tracking and Navigation: Theory Algorithms and Software. John Wiley and Sons: Inc, 2001.
39. Vrooijink GJ, Abayazid M, Patil S *et al.* Needle path planning and steering in a three-dimensional non-static environment using two-dimensional ultrasound images. *Int J Robot Res June* 2014; **33**: 1361–1374.
40. Patil S, Alterovitz R. Interactive motion planning for steerable needles in 3d environments with obstacles. Proceedings of IEEE RAS and EMBS International Conference on Biomedical Robotics and Biomechatronics (*BioRob*), Tokyo, Japan, 2010; 893–899.
41. Patil S, Burgner J, Webster RJ, III, Alterovitz R. Needle steering in 3-D via rapid replanning. *IEEE Transactions on Robotics August* 2014; **30**: 853–864.
42. LaValle SM. Planning Algorithms. Cambridge University Press, 2006.
43. Cholewiak RW, Collins AA. Sensory and physiological bases of touch *The Psychology of Touch* Heller MA, Schiff W (eds). Laurence Erlbaum Associates, 1991; 13–60.
44. Kaczmarek KA, Webster JG, Bach-y Rita P, Tompkins WJ. Electrotactile and vibrotactile displays for sensory substitution systems. *IEEE Transactions on Biomedical Engineering* 1991; **38**: 1–16.
45. Pongrac H. Vibrotactile perception: examining the coding of vibrations and the just noticeable difference under various conditions. *Multimedia Systems* 2008; **13**: 297–307.
46. Wallenstein S, Zucker CL, Fleiss JL. Some statistical methods useful in circulation research. *Circ Res* 1980; **47**: 1–9.
47. Garg A, Siauw T, Berenson D *et al.* Robot-guided open-loop insertion of skew-line needle arrangements for high dose rate brachytherapy. *IEEE Transactions on Automation Science and Engineering October* 2013; **10**: 948–956.

Supporting information

Additional supporting information may be found in the online version of this article at the publisher's web site.